Molecular Crystals and Liquid Crystals
Publication details, including instructions for authors and subscription information:
http://www.tandfonline.com/loi/gmcl20

Wave Mixing in Dye-Doped Chiral Nematics

D. Wei [a b], S. Residori [a] & U. Bortolozzo [a]

[a] INLN, Université de Nice-Sophia Antipolis, CNRS, Valbonne, France

[b] Department of Electronic Engineering, Xiamen University, Xiamen People's, Republic of China

Published online: 02 Apr 2013.

To cite this article: D. Wei, S. Residori & U. Bortolozzo (2013) Wave Mixing in Dye-Doped Chiral Nematics, Molecular Crystals and Liquid Crystals, 573:1, 54-63, DOI: 10.1080/15421406.2013.763337

To link to this article: http://dx.doi.org/10.1080/15421406.2013.763337

Mol. Cryst. Liq. Cryst., Vol. 573: pp. 54–63, 2013

ISSN: 1542-1406 print/1563-5287 online
DOI: 10.1080/15421406.2013.763337

Taylor & Francis
Taylor & Francis Group

Wave Mixing in Dye-Doped Chiral Nematics

D. WEI,[1,2] S. RESIDORI,[1] AND U. BORTOLOZZO[1]

[1]INLN, Université de Nice-Sophia Antipolis, CNRS, Valbonne, France
[2]Department of Electronic Engineering, Xiamen University, Xiamen People's Republic of China

Two-wave mixing (TWM) in nematic liquid crystals (LC) doped with azo-dyes and chiral agents that induce an helical structure is studied. Photo-induced changes of the cholesteric liquid crystal reflective band-gap are observed. The photo-induced spatial modulation of the chiral structure shows relatively fast response time and large nonlinearity. We have characterized the dependency of the nonlinear gain function on the different experimental parameters. It is also shown that the group velocities of light pulses can be decelerated dramatically in dye-doped cholesteric liquid crystal through TWM performed with a continuous pump and a time modulated signal. The highly dispersive properties of the medium can be exploited in interferometric sensors.

Keywords Azo-dyes; chiral nematics; holographic gratings; photo-isomerization; slow-light

1. Introduction

Chiral nematic liquid crystals (CLC) have recently attracted a large interest for photonics applications. Characterized by a self-assembled helical structure of their molecular arrangement, CLC show unique optical properties, such as selective Bragg reflection for circularly polarized light [1]. The distance that it takes for the nematic molecules to complete one turn (360°) is called the pitch P, whose structure is shown in Fig. 1(a). Induced by the periodic variation of the dielectric tensor, the reflective band-gap is determined by the helical pitch P of the chiral structure, that is, Bragg reflection occurs when the wavelength of the incident light is in the range $n_0P < \lambda < n_eP$, where n_0 and n_e are the ordinary, respectively, extraordinary refractive index of the liquid crystal (LC) medium.

Figure 1(b) shows a dye-doped nematic LC cell, 25 μm thickness, under polarized microscope in the reflection mode. The nematic mixture components are E7 (from Merck) and 0.5% of the azo-dye Methyl Red (MR). For comparison, in Figs. 1(c) and (d) are shown two pictures acquired under similar conditions but adding a chiral dopant, CB15, to the mixture. The Bragg reflection modes of two different concentrations of the chiral dopant can be appreciated by the change from red to the green spectrum in the reflected colors. The cells, 25 μm thickness, are filled with a chiral mixture whose components are E7, 0.5% MR, and respectively, 36.7% CB15 in Fig. 1(c) (mixture 2) and 40.3% CB15 in Fig. 1(d) (mixture 3). The helical pitch has been estimated to be $P \simeq 390$ nm in (c) and P

*Address correspondence to D. Wei, INLN, Institut Non Linéaire de Nice, Université de Nice-Sophia Antipolis, CNRS, 1361 route des Lucioles, 06560 Valbonne, France. E-mail: dong.wei@inln.cnrs.fr

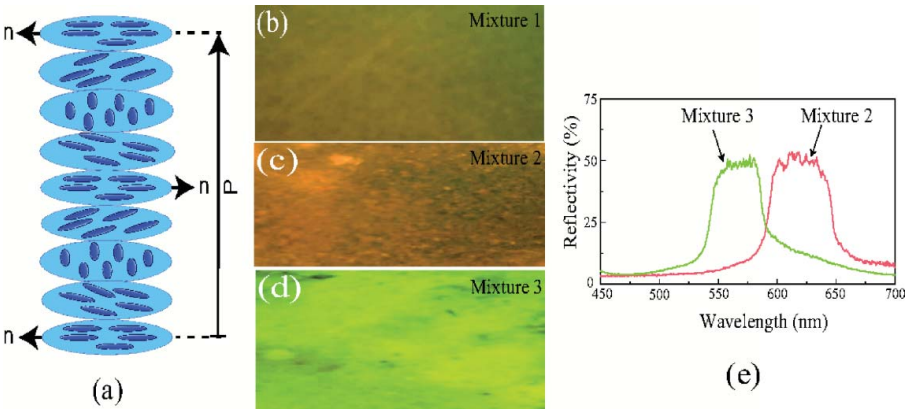

Figure 1. (a) Helical structure of a chiral nematic; *n* is the nematic director, *P* the helical pitch. (b–d) Reflection modes of dye-doped nematic LC under polarized microscope, whose mixture components are (b) E7 and 0.5% MR without chiral dopant, (c) E7, 0.5% MR and 36.7% CB15, (d) E7, 0.5% MR and 40.3% CB15. Bragg reflections in the red, respectively, green region of the spectrum correspond to the selective reflection bands shown in (e).

$\simeq$ 360 nm in (d). In Fig. 1(e) are shown the selective reflection band spectra corresponding to the mixtures of Figs. 1(c) and (d), respectively. An important parameter for CLC is the helical twisting power (HTP), which is related to the helical pitch P by the expression HTP $= 1/(P{\cdot}C)$, where C is the concentration of the chiral dopant. The HTP defines the ability of the chiral group to induce cholesteric mesomorphism in the nematic. Supposed that the HTP has a constant value, the helical pitch is varied with different concentrations of the chiral dopant.

The selective properties of dye-doped CLC, combined with the ability to change their pitch, for instance, with electric or magnetic fields, with temperature [2] or with light [3], allow attractive applications as frequency tunable lasers [4]. On the other hand, nematic LC exhibit huge nonlinearity when doped with a small amount of the MR azo-dye [5–7]. One of the main features of the MR is that, under the action of light, it can change its molecular conformation. The process is called photo-isomerization [8], and there are two isomers that are called the *trans* and *cis* form [9]. In the *trans* state, the molecules are more rod-like and aligned in the same direction, while in the *cis* state, the molecules become more isotropic and insensitive to the alignment of the surrounding LC. Azobenzene MR molecules go from the *trans* state to the *cis* one by absorbing a photon. Thermal relaxation brings them back to the *trans* form. Another important feature of MR molecules is their large dichroism, that is, light absorption is much higher along the molecular axis than it is in the transverse direction. As a consequence, molecules oriented in the direction of the light polarization are more likely to absorb a photon and undergo photo-isomerization. This property makes azobenzenes highly attractive for the design of rewritable photoresponsive optical elements [10,11]. The azobene *trans*-to-*cis* conformational change of the dye is responsible for a largely increased beam-coupling [12].

In our two-wave mixing (TWM) experiment, we fix the lower edge of the reflection band close to the absorption spectrum of the MR dye and show that, under these conditions, it is possible to obtain photo-induced effects on the chiral structure, thus providing a mechanism for efficient grating formation [13]. We demonstrate gain for the signal beam, with a relatively fast response time. The process and its gain features are characterized as a function of the different TWM parameters, such as pump to signal beam intensity ratio

β and fringe period Λ. Dye-doped CLC combine selective reflection with high nonlinearity, hence, exhibit novel features of wave-mixing. They also achieve a big change of the group velocity, which is described as "slow- and fast-light" effects [14]. Many slow- and fast-light schemes were proposed and experimentally realized based on different effects, such as electromagnetically induced transparency (EIT) [15], coherent population oscillations (CPO) [16,17], stimulated Brillouin, and Raman scattering [18–22], TWM in photorefractive crystals [23–25] and in nematic LC [26–28]. The slow-light through TWM in dye-doped CLC is observed without voltage applied, and the group velocity can reach, in our experiment, values as small as 0.75 mm s^{-1}. Recently, slow-light in dye-doped CLC was also obtained in four-wave mixing configuration, leading to phase conjugation [29].

2. Experimental Setup

The dye-doped CLC mixture consists of a nematic LC host, E7, doped with a small amount, 0.5% in weight, of the MR and with 36.7% in weight of the chiral nematic CB15. The mixture is injected in between two planar rubbed polyvinyl alcohol-coated glass plates with 25 μm thick spacers. The CLC cell is covered with thin "homogeneous (planar) alignment" PVA layer. Therefore, the alignment layers of the CLC cell force the mesogenic molecules to line up with their long molecular axis parallel to the alignment layer and, thus, parallel to the glass plates of the cell. Therefore, the helical structure spontaneously arranges perpendicularly to the rubbing direction. The reflective spectrum of the filled cell is measured by exposing the sample at a collimated white light and by using a spectrometer. The result is shown in Fig. 2(a). For comparison, the absorption spectrum of the MR in E7 is displayed on the same graph. The central wavelength λ_0 of the CLC reflection band is about 615 nm. Considering that $\lambda_0 = \bar{n}P$, where $\bar{n}$ is the average refractive index of the LC, we can estimate the pitch to be $\bar{n}P \simeq 390$ nm, with the region $n_oP < \lambda < n_eP$ defining the reflective band.

The experimental setup consists of a pump-probe scheme, as shown in Fig. 2(b). The wavelength of the writing beam is 532 nm, which is in the absorption spectra of the MR, so that the MR photo-isomerization is facilitated. The laser passes through neutral density filters that can be used to alter the intensity. Then, the laser beam is split into two writing beams with a beam splitter. The two beams are enlarged and collimated (transverse diameter

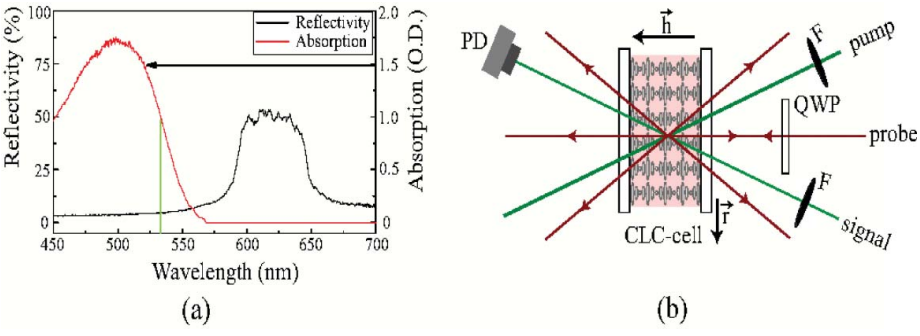

Figure 2. (a) Absorption spectrum of the MR in E7 (red curve) and reflection band of the CLC, 36.7% CB15 in E7, (blue curve); MR is 0.5% in both cases. (b) Experimental setup: $\vec{h}$ is the wave vector of the helical structure and $\vec{r}$ is the rubbing direction; QWP: quarter-wave plate; F: neutral density filter; PD: photodiode. From [13].

3 mm) and, then, sent to interfere onto the cell. The two writing beams, called pump and signal, normally meet at the surface of the CLC cell. The interference intensity fringes give rise to refractive index differences in the medium, inducing a complex dynamical hologram in the medium [30]. The resulting grating wave vector amplitude is $k = 2\pi/\Lambda$. The fringe period Λ is given by $\Lambda = \lambda/(2\sin\theta)$, where λ is the pump and signal beam optical wavelength, and θ is the pump E_P and signal E_S incidence angle with respect to the normal of the CLC cell. To probe the refractive index change, we used a linearly polarized low-power red laser with wavelength 632.8 nm.

Quarter-wave plates (QWP) are placed before the cell and used to independently to control the polarization state of each input beam. The neutral density filter placed in the arms of the interferometer can modulate the parameter pump-to-signal intensity ratio β, which is defined as $\beta = |E_P|^2/|E_S|^2$, where $|E_P|^2$ and $|E_S|^2$ are measured by a power meter.

2.1 Spectral Properties and Photo-Isomerization

Before performing TWM, the photo-induced change of the cholesteric liquid crystal reflective band-gap is studied. We illuminate the cell with white light and record its reflection band by using a spectrometer. Simultaneously, a pump beam is sent onto cell and overlapped with the white beam. The white beam size has to be smaller than the pump beam. Under illumination from the pump beam, a slight displacement of the right band-edge can be appreciated, while the left band-edge does not change. This behavior confirms the role of the dyes in yielding a decrease of the refractive index anisotropy via photo-isomerization processes. The shift of the right band-edge of the spectrum is shown in Fig. 3(a), where the spectrum recorded without the pump is compared with those recorded under different pump intensities.

The right band-edge λ_R (determined at half-height), which is equivalent to n_eP, is plotted in Fig. 3(b) versus the incident pump intensity I. The behavior of λ_R is fitted by using a phenomenological dependence on the illuminating intensity I, which can be expressed as $\lambda_R(I) = \lambda_{R1} + \lambda_{R2}\exp(-\alpha I)$, with $\lambda_R(0) = \lambda_{R1} + \lambda_{R2}$ the dark value and α the efficiency of the trans-cis photo-isomerization of the dye [31]. By using this formula, a best fit is obtained for $\lambda_{R1} = 613.09$ nm, $\lambda_{R2} = 8.34$ nm and $\alpha = 0.0043$, therefore, $\lambda_R(0) = \lambda_{R1} + \lambda_{R2} = 621.8$ nm. This mechanism catches the essential of the photo-isomerization process inducing the grating formation that will be described in the following

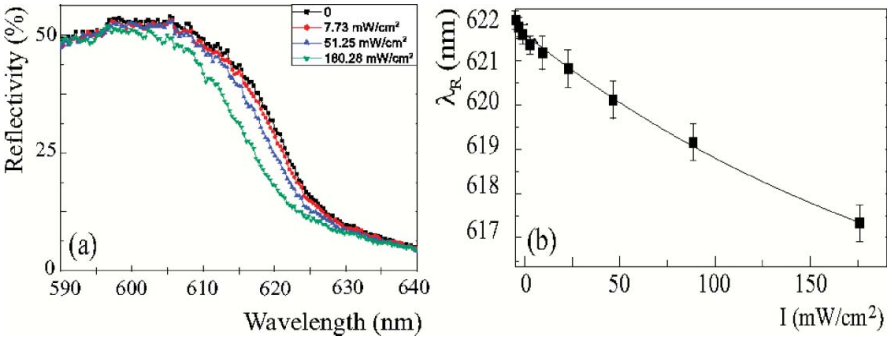

Figure 3. (a) Right side of the reflective spectra measured at different illumination powers. (b) Right band-edges λ_R (squares) versus the pump intensity; the solid line is a best fit with the theoretical expression for the effective shift of the right-reflective bands.

section. Indeed, the illumination at 532 nm induces a small change of the medium birefringence, as reflected by the small shrinks of the reflective band. Correspondingly, in TWM, the pump and signal beams experience in the bright and, respectively, dark regions different refractive indices [32].

3. Two-Beam Coupling: Experimental Results

After having characterized the spectral properties of the dye-doped CLC mixture, we perform TWM. The setup is shown in Fig. 2(b). The CLC cell is illuminated by a pump and a signal beams, which lead, in the interference region, to the following intensity distribution

$$|E_{\text{in}}|^2 = |E_S|^2 + |E_P|^2 + 2E_S E_P \cos(qx), \tag{1}$$

where $q = 2\pi/\Lambda$ is the grating wave vector, Λ is the fringe period, and x is the coordinate along the grating.

Nonlinear wave-mixing in thin media implies coupling in the Raman–Nath regime of optical diffraction, which produces several output order beams [33]. As a first set of measurements, the TWM is performed with linearly polarized pump and signal. The intensities $I_P = |E_P|^2$ and $I_S = |E_S|^2$ of the pump, respectively, signal beam are taken equal, $I_P = I_S = 4.46$ mW cm^{-2}, and $\Lambda = 15.2$ μm. Depending on the probe polarization, which is controlled by a QWP, reflected or transmitted orders of the probe beam are observed. The grating is tested by measuring the intensity I_1 of the first diffracted order both on the reflected and transmitted probe. The corresponding diffraction efficiencies, $\eta = I_1/I_S$, are plotted in Fig. 4(a) as a function of the probe polarization (the angle of the QWP is measured with respect to $\vec{r}$).

A maximum diffraction efficiency is observed on the transmitted probe when the polarization is left circular, while a maximum diffraction is obtained on the reflected probe for a right circular polarization. These polarization features are consistent with the chiral structure of the CLC. Indeed, since the probe wavelength is inside the reflective band of our mixture, we expect light of the same handedness of the helix to be reflected while the component of opposite handedness is expected to be transmitted [1]. Similar values of η are obtained for any linear polarization of the two interacting beams, indicating that

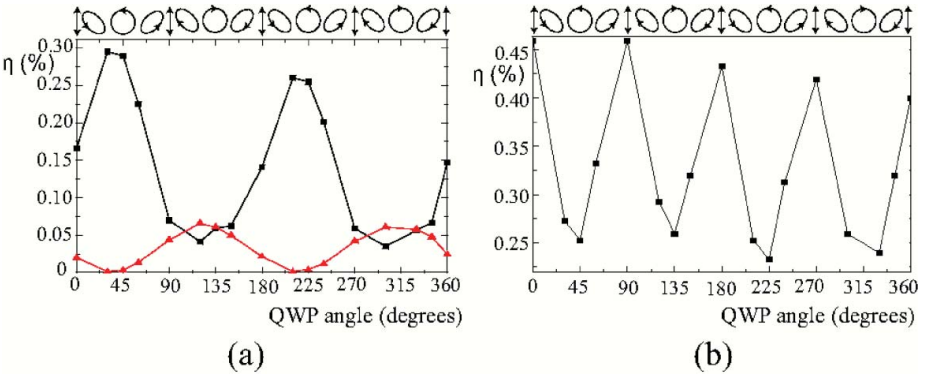

Figure 4. First-order probe diffraction efficiency versus its polarization state for (a) a dye-doped chiral nematic LC, (b) a dye-doped nematic LC without chiral dopant. Black square: transmitted first-order; red triangle: reflected first-order.

the photo-induced grating formation preserves the chiral structure. This confirms previous observations of grating formation in dye-doped chiral nematics [34].

The handedness of the helix inside the CLC layer is independently determined by uniformly illuminating the cell with a collimated white light and, then, analyzing the polarization state of the reflected light with a QWP and a polarizer in sequence. The result is that the CLC is right-handed, which is in agreement with the observation of maximum η on the transmitted (reflected) beam for a left-circular (right-circular) probe, respectively.

Since the photo-isomerization reaction of the azo-dye affects the alignment of the LC molecules, spatial distribution of the molecular reorientation are induced by irradiation with polarized interference light. It was shown that the reconstructing properties of polarization holograms that are recorded in the azo-dye-doped nematic LC are strongly dependent on the initial alignment of the LC [35,36]. For TWM in dye-doped CLC the diffraction efficiency is optimized for circular polarization of the interacting beams [13].

For comparison, the behavior of the probe diffraction efficiency in azo-dye-doped nematic LC without chiral dopant is also studied. A new cell, whose mixture is composed of the nematic LC E7 and 0.5% MR without chiral dopant, is used to replace the CLC cell in the setup of Fig. 2. The dependency of the transmitted first-order diffraction efficiency on the polarization state of the probe beam is shown in Fig. 4(b). At variance with the CLC cell, the maximum diffraction efficiency is obtained for linear polarization, while minimum diffraction efficiency is observed for circularly polarized probe.

3.1 Response Time

Then, we return back to the study of the CLC properties. In order to characterize the typical response time of the medium, self-diffraction experiments are performed with equal intensities of the two writing beams $I_P = I_S$, the probe beam removed and $\Lambda = 7.7$ μm. The intensity of the first diffraction order of the signal beam, called I_{out}, is measured with a photodiode, while the pump beam is switched on/off by a chopper (frequency 2 Hz).

A typical time behavior of the I_{out} output beam is shown in Fig. 5. A relatively short rise time, ~25 ms for a pump power $P_p \sim 5$ mW [13], is observed. It can be attributed to a photo-induced, and dye-mediated deformation of the chiral structure. Periodic photo-isomerization of the MR can induce refractive index modulation via molecular reorientation in the nematic host [37] or via change of the LC order parameter [38]. The fall time

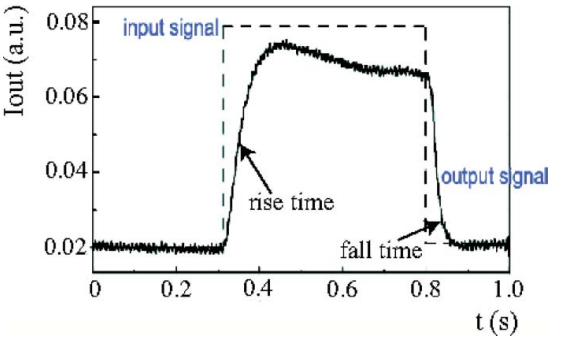

Figure 5. Time behavior of the output I_{out} beam by switching on/off the pump beam (dashed line); left-circular polarization and 1.4 mW total power.

$\sim$10 ms [13], is mainly due to diffusion of excited dye molecules [39,40]. It can, thus, be taken as

$$\tau_{\text{fall}} = \frac{1}{D\left(\frac{4\pi^2}{\Lambda^2}\right) + (1/T_{\text{cis}})}, \tag{2}$$

where D is the diffusion coefficient of the dye molecules along $\vec{r}$, Λ is the fringe period and T_{cis} is the lifetime of the *cis* state in the presence of the host molecules [37].

3.2 Gain Features

During the TWM process, the two writing beams are diffracted by the same index grating that they have induced in the CLC cell. The intensity I_{out} of the output signal was measured in the far-field of the diffracted beam. To measure the gain, a 1-mm-diameter pinhole was used to separate the transmitted signal from the pump beam. In the Raman–Nath regime of diffraction, that is, for $\Lambda > d$, and far from saturation effects, the TWM gain can be expressed as [30,41]

$$G = \frac{I_{\text{out}}(\text{with the pump})}{I_{\text{out}}(\text{without the pump})} = 1 + \left[\frac{2\pi}{\lambda} n_2 I_P\right]^2 d^2, \tag{3}$$

where n_2 is the Kerr-like coefficient of the medium that is, the slope of the refractive index change versus the intensity, and d is the cell thickness.

In Fig. 6(a), the measured G is plotted as a function of $\beta = I_P/I_S$, for a grating spatial period $\Lambda = 15.34$ μm and for pump and signal either both linearly polarized or both left-circularly polarized. When increasing the pump intensity from 4.46 mW cm^{-2} to 14.57 mW cm^{-2}, the maximum gain rises from 1.74 to 2.78, respectively. The results fit Eq. (3) quite well. For the same pump intensity, the gain obtained with left-circularly polarized beams is slightly higher than that obtained with linear pumps. Consistently with the right-handed helical structure of the CLC, we can interpret this result by considering that an optimal

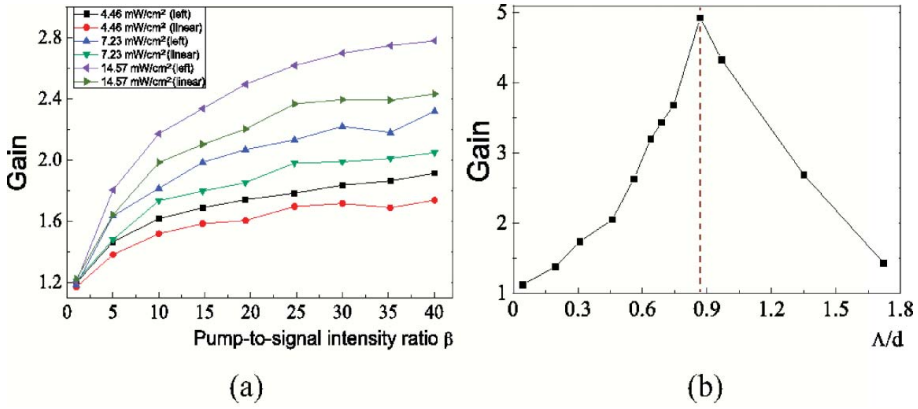

Figure 6. (a) TWM gain as a function of β; $\Lambda = 15.34$ μm. (b) TWM gain as a function of the grating period Λ; $\beta = 30$. From [13]

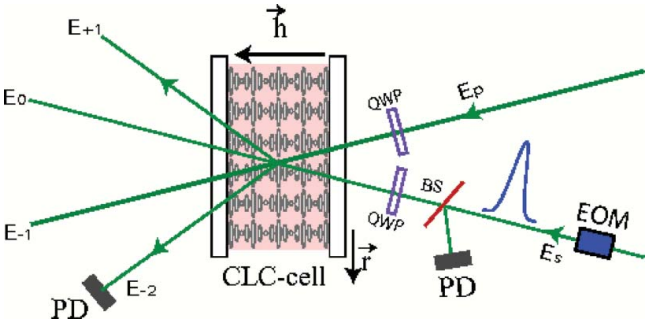

Figure 7. Experimental setup for slow-light through wave-mixing in the dye-doped chiral cell. EOM: electro-optic modulator; BS: beam splitter.

coupling with the photo-induced grating is realized for left-circularly polarized beams even when wavelengths are outside the reflective band-gap.

The G is measured as a function of the grating period Λ as well. The results are plotted in Fig. 6(b) for $\beta = 30$ and $I_P = 14.57$ mW cm^{-2}. We see that a maximum gain, $G = 5$, is obtained as $\Lambda \cong d$. From the maximum observed gain, by using the expression valid in the Raman–Nath regime of diffraction, Eq. (3), we can estimate a nonlinear coefficient of approximately $n_2 \cong 0.5$ cm^2 W^{-1}.

3.3 Slow-Light

Finally, slow-light through TWM is demonstrated by performing two-beam coupling experiments with a continuous pump E_P and a time modulated signal beam E_S. As shown in Fig. 7, the previous setup (Fig. 2(b)) is modified by adding an electro-optic modulator (EOM) on the path of the signal beam. By appropriate driving of the EOM, the signal is shaped with a Gaussian temporal profile.

The temporal envelopes of the input signal beam E_S, obtained before the CLC cell, and of the normalized –2 output order pulse E_{-2} are recorded with a photo-diode (PD) as a

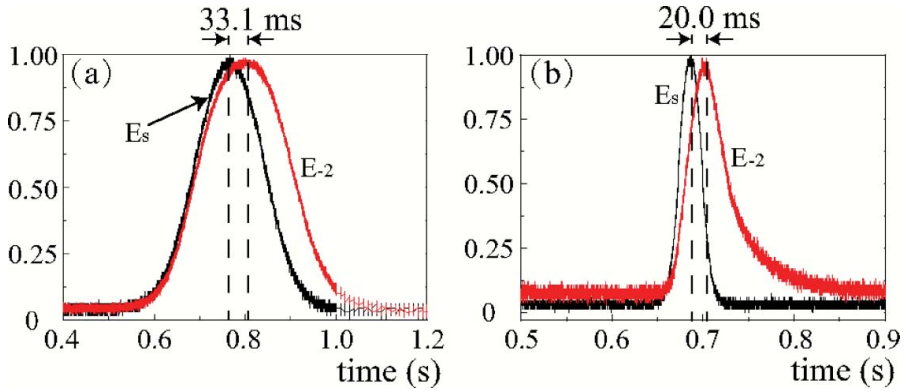

Figure 8. Experimental time dependencies of the –2 output order pulse E_{-2} (red line) and of the input pulse E_S (black line); (a) $t_0 = 170.7$ ms, (b) $t_0 = 28.1$ ms. The pulse heights are normalized to their respective maximum in order to facilitate the comparison of the input and output pulse shapes.

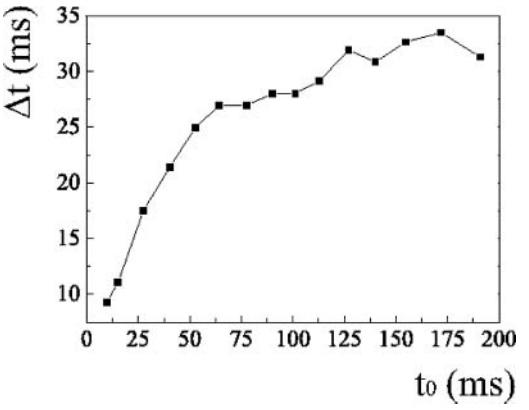

Figure 9. The group delay Δt measured on the –2 output order pulse versus the input pulse width t_0.

function of different t_0, where t_0 is the half-width of the input pulse. In this paper, we focus on the behavior of the output order $m = -2$ since it is showing the largest slow-light delay in the experiment. Indeed, it has been shown that in Raman–Nath regime the maximum group delay is on the –2 order [26]. Two examples of experimental time dependencies of the input pulse E_S (black line) and of the –2 output order pulse E_{-2} (red line) are shown in Fig. 8. The width of the input pulse was $t_0 = 170.7$ ms in Fig. 8(a) and $t_0 = 28.1$ ms in Fig. 8(b). We can note that, as the input pulse width decreases, the output pulse undergo distortion effects due to the finite frequency bandwidth of the TWM process. The group delay Δt between the output pulse E_{-2} and the input pulse E_S can be estimated by comparing the respective positions of the output and input pulse peaks. We obtain 33.1 ms in Fig. 8(a) and 20.0 ms in Fig. 8(b).

In Fig. 9, the group delay Δt is plotted as a function of t_0. In the Raman–Nath regime, and for the –2 diffraction order, we have obtained a maximum group delay of 33.5 ms. Correspondingly, the group velocity of the pulse can be estimated by using the expression $\upsilon_g \equiv d/\Delta t$. The lowest achieved group velocity is calculated to be as small as 0.75 mm s^{-1}.

4. Conclusions

We have demonstrated beam coupling in dye-doped chiral nematics, with a relatively fast response time, maximum gain for circularly polarized pumps and no external voltage applied. In the same system, slow-light can be obtained by exploiting the dispersion properties associated with the beam coupling when one of the two interacting beams is shaped as a temporal pulse. The large dispersive properties of the medium lead to the achievement of a very low group velocity and can be exploited for the realization of interferometric sensors.

Acknowledgments

We acknowledge A. Iljin and Z. Cai for helpful discussions. D. Wei acknowledges financial support from the China Scholarship Council.

References

[1] de Gennes, P. G., & Prost, J. (1993). *The Physics of Liquid Crystals*, Oxford Science Publications.

[2] Chilaya, G., Bahr, Ch., and Kitzerow, H. (2000). *Cholesteric Liquid Cystals: Optics, Electrooptics and Photooptics in Chirality in Liquid Crystals*, Springer Verlag: New York.
[3] Boychuk, V., Gerus, I., ljin, A. I., & Parka, J. (2009). *Opto-Electronics Rev.*, *17*, 287.
[4] Coles, H., & Morris, S. (2010). *Nature Photonics*, *4*, 676.
[5] Khoo, I. C., Slussarenko, S., Guenther, B. D., Shih, M.-Y., Chen, P., & Wood, W. V. (1998). *Opt. Lett.*, *23*, 253.
[6] Simoni, F., Lucchetti, L., Lucchetta, D. E., & Francescangeli, O. (2001). *Opt. Express*, *9*, 85.
[7] Khoo, I. C. (2009). *Phys. Rep.*, *471*, 221.
[8] McConville, S., Laurent, D., Guarino, A., & Residori, S. (2005). *Am. J. Phys.*, *73*, 425.
[9] Simoni, F., & Francescangeli, O. (1999). *J. Phys.: Condens. Matter*, *11*, R439.
[10] De Sio, L., Ferjani, S., Strangi, G., Umeton, C., & Bartolino, R. (2011). *Soft Matter*, *7*, 3739.
[11] Gilardi, G., De Sio, L., Beccherelli, R., Asquini, R., d!¯Alessandro, A., & Umeton, C. P. (2011). *Opt. Lett.*, *36*, 4755. Oxford Science Publications: England.
[12] Petrossian, A., and Residori, S. (2003). *Opt. Commun.*, *228*, 145.
[13] Wei, D., Iljin, A., Cai, Z., Residori, S., &Bortolozzo, U. (2012). *Opt. Lett.*, *37*, 734.
[14] Boyd, R. W., & Narum, P. (2007). *J. Mod. Optics*, *54*, 2403.
[15] Fleischhauer, M., Imamoglu, A., & Marangos, J. P. (2005). *Rev. Mod. Phys.*, *77*, 633.
[16] Bigelow, M. S., Lepeshkin, N. N., & Boyd, R. W. (2003). *Phys. Rev. Lett.*, *90*, 113903.
[17] Palinginis, P., Sedgwick, F., Crankshaw, S., Moewe, M., & Chang-Hasnain, C. J., (2005). *Opt. Express*, *13*, 9909.
[18] Song, K. Y., Herráez, M. G., González, M., & Thévenaz, L. (2005). *Opt. Lett.*, *30*, 1782.
[19] Stenner, M. D., Nedfield, M. A., Zhu, Z., Dawes, A. M. C., & Gauthier, D. J. (2005). *Opt. Express*, *13*, 9995.
[20] Okawachi, Y., Bigelow, M. S., Sharping, J. E., Zhu, Z., Schweinsberg, A., Gauthier, D. J., Boyd, R. W., & Gaeta, A. L. (2005). *Phys. Rev. Lett.*, *94*, 153902.
[21] Sharping, J., Okawachi, Y., & Gaeta, A. (2005). *Opt. Express*, *13*, 6092.
[22] Dahan, D., & Eisenstein, G. (2005). *Opt. Express*, *13*, 6234.
[23] Podivilov, E., Sturman, B., Shumelyuk, A., & Odoulov, S. (2003). *Phys. Rev. Lett.*, *91*, 083902.
[24] Shumelyuk, A., Shcherbin, K., Odoulov, S., Sturman, B., Podivilov, E., & Buse, K. (2004). *Phys. Rev. Lett.*, *93*, 243604.
[25] Zhang, G., Dong, R., Bo, F., & Xu, J. (2004). *Appl. Opt.*, *43*, 1167; Zhang, G., Bo, F., Dong, R., & Xu, J. (2004). *Phys. Rev. Lett.*, *93*, 133903.
[26] Residori, S., Bortolozzo, U., & Huignard, J. P. (2008). *Phys. Rev. Lett.*, *100*, 203603.
[27] Bortolozzo, U., Residori, S., & Huignard, J. P. (2010). *Laser Photonics Rev.*, *4*, 483.
[28] Residori, S., Bortolozzo, U., & Huignard, J. P. (2009). *Appl. Phys.* B, *95*, 551.
[29] Wei, D., Residori, S., & Bortolozzo, U. (2012). *Opt. Lett.*, *37*, 4684.
[30] Brignon, A., Bongrand, I., Loiseaux, B., & Huignard, J. P. (1997). *Opt. Lett.*, *22*, 1855.
[31] Iljin, A., Reshetnyak, V., Shelestiuk, S., & Yarmolenko, V. (2006). *Mol. Cryst. Liq. Cryst.*, *453*, 263.
[32] Yang, D.-K., & Wu, S.-T. (2006). *Fundamentals of Liquid Crystal Devices, Wiley-SID Series in Display Technology*, Wiley: Hoboken,.
[33] Yariv, A. (2003). *Optical Waves in Crystals*, John Wiley: New Jersey, pp. 354–358.
[34] Sasaki, T., Emoto, A., Shioda, T., & Ono, H. (2009). *Appl. Phys. Lett.*, *94*, 023303.
[35] Hrozhyk, U. A., Serak, S. V., Tabiryan, N. V., & Bunning, T. J. (2007). *Adv. Mater. (Weinheim, Ger.)*, *17*, 1735.
[36] Sasaki, T., Ono, H., & Kawatsuki, N. (2008). *Appl. Opt.*, *47*, 2192.
[37] Sabet, R. A., Khoshsima, H. (2010). *Dye and Pigments 87*, 95.
[38] Iljin, A. (2011). *Mol. Cryst. Liq. Cryst. 543*, 143.
[39] Rudenko, E. V., & Sukhov, A. V. (1994). *JETP 78*, 875.
[40] Khoo, I. C. (1996). *IEEE J. Quantum Electron 32*, 525.
[41] Gunter, P., & Huignard, J. P. (2006). *Photorefractive Materials and Their Applications 1*, Springer Science: New York.